Journal of Electroanalytical Chemistry 643 (2010) 20–30

Contents lists available at ScienceDirect

Journal of Electroanalytical Chemistry

journal homepage: www.elsevier.com/locate/jelechem

Facilitated anion transfer reactions across oil|water interfaces

S.A. Dassie *

Instituto de Investigaciones en Fisicoquímica de Córdoba (INFIQC), Departamento de Fisicoquímica, Facultad de Ciencias Químicas, Universidad Nacional de Córdoba, Ciudad Universitaria, X5000HUA Córdoba, Argentina

ARTICLE INFO

Article history:
Received 6 December 2009
Received in revised form 9 March 2010
Accepted 11 March 2010
Available online 15 March 2010

Keywords:
Digital simulation
Facilitated anion transfer
Water autoprotolysis
Liquid|liquid interface
Coupled chemical reaction

ABSTRACT

In this paper we present the general equations for a model of anion transfer reactions across the oil|water interface assisted by a neutral ligand. Our analysis mainly focuses on the effect of water autoprotolysis. The equations reported here allow us to simulate the system under a variety of possible conditions. The formation of complex with *j*:*k* anion-to-ligand stoichiometry is analyzed. Three different models are compared: buffered solutions (BASA model) and unbuffered solutions with and without considering water autoprotolysis (UBASA and UBAS model respectively). Moreover, the analytical relationships for the BASA model between half-wave potential and the initial concentration of anion and ligand are developed.

1. Introduction

Different assisted ion transfer mechanisms have been studied and published since Koryta [1] reported that a decrease in the Gibbs energy of transfer of an ion could be found due to the formation of a complex with a ligand or ionophore [2].

The molecular recognition of anions has received in recent years special attention in the areas of supramolecular chemistry and analytical chemistry [3]. During the last decade, the facilitated anion transfer across the ITIES (interface between two immiscible electrolyte solutions) was researched extensively using electrochemical techniques. Assisted anion transfer has been analyzed for different anions in different solvents [4].

Shao et al. studied the complex formation between the synthetic dicarboxylate receptor *para*-xylylenyl-bis-(iminoimidazolinium) and dicarboxylates and analyzed its effect on the anion transfer across a water|nitrobenzene (W|NB) interface [5]. Lately, Shao and co-workers used electrochemical methods to study the thermodynamic and the kinetic transfer behaviour of several monovalent anions, Cl^-, Br^-, NO_2^- and CH_3COO^-, at a micro-water|1,2-dichloroethane (W|1,2-DCE) interface. In this case, the anion transfer was assisted by β-octafluoro-*meso*-octamethylcalix[4]pyrrole [6].

Teramae and co-workers reported the facilitated transfer of various hydrophilic anions across W|1,2-DCE and W|NB interfaces [4]. The facilitated transfer of sulfate has been reported using strong hydrogen-bonding ionophores across a polarized W|1,2-DCE [7] and W|NB [8] interface. The selective transfer of HPO_4^{2-} and $H_2PO_4^-$ across a W|NB interface has also been reported using a thiourea-based hydrogen-bond forming ionophore consisting of a xylene unit [9], and using a thiourea–isothiouronium conjugate [10] or a thiourea-functionalized benzo-15-crown-5 [11] for selective binding of $H_2PO_4^-$ at the W|1,2-DCE interface. Nishizawa et al. [12] studied the transfer of hydrophilic anions across the liquid–liquid interface assisted by bis-thiourea ionophore. These authors demonstrated that a hydrogen-bond forming bis-thiourea can effectively facilitate the transfer of various hydrophilic anions, such as Cl^-, CH_3COO^-, $H_2PO_4^-$, HPO_4^{2-} and SO_4^{2-}, across the W|NB interface. In addition, the chloride transfer across the W|NB interface assisted by a mono-thiourea ionophore was characterized using ion transfer polarography [13].

Qian et al. [14] recently designed a micro-ITIES array for the detection of nitrate by facilitated ion transfer by a neutral tripodal amide-based ionophore, *N*-{2-[bis-[2-(4-*t*-butylbenzoylamino)ethyl]amino]ethyl}-4-*t*-butylbenzamide. The complexation between this neutral tripodal amide-based ionophore and three adenosine-containing nucleotides, ATP, ADP, and AMP, was investigated by facilitated ion transfer processes through a microhole array film at the W|1,2-DCE interface [15].

Dryfe et al. [16] studied the facilitated transfer of halide anions (F^-, Cl^- and Br^-) across a polarized W|1,2-DCE interface using steroid-based cholapod receptors. The transfer of F^- ion assisted by an organometallic complex cation tetraphenylantimony across the polarized W|NB interface has taken place by means of ion transfer voltammetry [17].

* Tel./fax: +54 351 4334188.
E-mail address: sdassie@mail.fcq.unc.edu.ar

1572-6657/$ - see front matter © 2010 Elsevier B.V. All rights reserved.
doi:10.1016/j.jelechem.2010.03.013

Rodgers et al. [18] reported an electrochemically controlled molecular recognition of heparin using the synthetic heparin mimetic Arixtra at W|NB microinterfaces assisted by quaternary ammonium ionophores. More recently, Kivlehan et al. [19] reported a complete analysis of the interaction of a urea-functionalized calix[4]arene ionophore using voltammetric ion transfer at the W|1,2-DCE interface and a combination of nuclear magnetic resonance (NMR) spectrometry and potentiometric selectivity coefficient evaluation. Boronic acid-facilitated α-hydroxy-carboxylate anion transfer at liquid|liquid electrode systems has been analyzed by Katif et al. [20]. The transfer of the α-hydroxy-carboxylates of glycolic, lactic, mandelic and gluconic acid from the aqueous electrolyte phase into an organic 4-(3-phenylpropyl)-pyridine phase was studied at a triple-phase boundary electrode system.

Different anion-to-ligand stoichiometries for several systems have been reported in the literature, namely 1:1 [5–20], 1:2 [8] and 2:1 [9]. In the last case it was suggested that the ligand promotes interaction between $H_2PO_4^-$ anions [4,9].

Cation transfer assisted by a ligand was reported in several experimental and theoretical works. After the pioneering work by Homolka et al. [21], where the authors performed digital simulations of the current–potential curves for the formation of complexes of different stoichiometry, numerical simulations of the voltammetric response for numerous mechanisms have been successfully carried out [22–33].

A theoretical approach for the proton facilitated transfer or protonable species transfer was studied by Reymond et al. [34]. They developed a theory of reversible transfer reactions for molecules containing an unlimited number of protonation–deprotonation sites that can cross the interface in all their ionic forms. Osakai and co-workers [35,36] deduced a theoretical equation for the polarographic current–potential profiles corresponding to the transfer of an oligopeptide or an amino acid at the oil|water interface, facilitated by a neutral ionophore. Dassie [37,38] derived the general equations for ion transfer reactions across the oil|water interface assisted by a protonatable neutral ligand. This model was solved using Laplace transforms and the explicit consideration of water autoprotolysis was analyzed. Finally, the last model was also solved by Garcia et al. [39] using explicit finite difference to account for the different diffusion coefficients of each species in each phase. This model was corroborated by the experimental results for the quinine transfer across the water|1,2-dichloroethane interface under different conditions [39].

In spite of the vast amount of information on the assisted transfer of cations across liquid|liquid interfaces, according to our knowledge, no theoretical treatment has been proposed in the literature for facilitated anion transfer. Experimental results, however, have already been published. In this work, the derivation of the general equations for anion transfer reactions across oil|water interface assisted by a neutral ligand is presented. The effect of water autoprotolysis on facilitated anion transfer is analyzed. The equations developed in this research allow simulating the system in different experimental conditions. The formation of three different interfacial complexes (with 1:1, 1:2 and 2:1 anion-to-ligand stoichiometry) is studied in detail.

1.1. Theory

In order to derive the current–potential equation for anion facilitated transfer by a neutral ligand, L, the following assumptions are made:

(a) The interface between the aqueous and the organic phase is stationary and planar.
(b) Both phases contain enough inert electrolytes so that migration of the transferring ion can be neglected.
(c) Complex formation and dissociation are at equilibrium even when current is flowing, as the rates of the complex formation and dissociation processes are sufficiently high compared with the corresponding diffusion rates.
(d) Acid–base association and dissociation are at equilibrium even when current is flowing, since the rates of the acid–base association and dissociation processes are sufficiently high in relation to the corresponding diffusion rates.
(e) Transfer of all species through the interface is reversible and diffusion-controlled. Diffusion occurs in the x coordinate, normal to the interface, defined at $x = 0$.
(f) Double-layer effects and adsorption are not considered in the model, and neither are acid dissociation constant and complex formation constant change between the bulk and the interface.
(g) The distribution constants of the neutral species, L and H_nP, do not depend on the applied potential and are defined as: $K_{D,L} = \frac{c_L^o}{c_L^w}$ and $K_{D,H_nP} = \frac{c_{H_nP}^o}{c_{H_nP}^w}$, respectively.
(h) All the charged species are perturbed by the potential applied to the interface and depend on the Nernst equation.
(i) The diffusion coefficients in each phase are the same for all species. This is acceptable for all species except for H^+ in the aqueous phase, but this assumption is necessary so as to apply Matsuda's approach to the model [24].
(j) In the BASA model, the total buffer concentration is larger than the total ligand concentration and sufficient to maintain a constant pH value.
(k) All activity coefficients are equal to one.
(l) The neutral species, H_nP, not form complexes with the neutral ligand.

The acid–base equilibriums of the H_nP are the following:

$$H_{(n-i)}P^{i-} \rightleftharpoons H^+ + H_{(n-i-1)}P^{(i+1)-}$$

the $(i+1)$-acid dissociation constant in the α-phase is defined by:

$$K_{a,(i+1)}^{\alpha} = \frac{c^{\alpha}_{H_{(n-i-1)}P^{(i+1)-}} c^{\alpha}_{H^+}}{c^{\alpha}_{H_{(n-i)}P^{i-}}} \quad (1)$$

for $i = 0, \ldots, n$ and α = organic phase (o) or aqueous phase (w). It is important to note that P^{n-} is the fully deprotonated species.

Water autoprotolysis is explicitly considered:

$$H_2O \rightleftharpoons H^+ + HO^-$$

and the water autoprotolysis constant is defined as follows:

$$K_w = c^w_{H^+} c^w_{HO^-} \quad (2)$$

All the anions can form complexes $j:k$ with the neutral ligand, which coexist in both phases. The neutral species H_nP does not form complex with the neutral ligand.

The *ijk*-complex formation equilibriums are the following:

$$jH_{(n-i)}P^{i-} + kL \rightleftharpoons \left[\left(H_{(n-i)}P\right)_j L_k\right]^{ji-}$$

and the *ijk*-overall formation constant in α phase is defined by:

$$\beta^{\alpha}_{ijk} = \frac{c^{\alpha}_{[(H_{(n-i)}P)_j L_k]^{ji-}}}{\left(c^{\alpha}_{H_{(n-i)}P^{i-}}\right)^j \left(c^{\alpha}_L\right)^k} \quad (3)$$

for $i = 1, \ldots, n$, $j = 1, \ldots, m$ and $k = 1, \ldots, l$.

The distribution of charged species at the interface is defined by the following Nernst equations:

$$\frac{c^{o}_{H_{(n-i)}P^{i-}}(0,t)}{c^{w}_{H_{(n-i)}P^{i-}}(0,t)} = \exp\left[-\frac{iF}{RT}\left(\Delta^{w}_{o}\phi - \Delta^{w}_{o}\phi^{o'}_{H_{(n-i)}P^{i-}}\right)\right] \quad \text{for } i = 1,\ldots,n \tag{4}$$

$$\frac{c^{o}_{[(H_{(n-i)}P)_jL_k]^{ji-}}(0,t)}{c^{w}_{[(H_{(n-i)}P)_jL_k]^{ji-}}(0,t)} = \exp\left[-\frac{jiF}{RT}\left(\Delta^{w}_{o}\phi - \Delta^{w}_{o}\phi^{o'}_{[(H_{(n-i)}P)_jL_k]^{ji-}}\right)\right] \tag{5}$$

for $i = 1,\ldots,n,\ j = 1,\ldots,m$ and $k = 1,\ldots,l$.

$$\frac{c^{o}_{H^+}(0,t)}{c^{w}_{H^+}(0,t)} = \exp\left[\frac{F}{RT}\left(\Delta^{w}_{o}\phi - \Delta^{w}_{o}\phi^{o'}_{H^+}\right)\right] \tag{6}$$

and

$$\frac{c^{o}_{HO^-}(0,t)}{c^{w}_{HO^-}(0,t)} = \exp\left[-\frac{F}{RT}\left(\Delta^{w}_{o}\phi - \Delta^{w}_{o}\phi^{o'}_{HO^-}\right)\right] \tag{7}$$

In Eqs. (4)–(7), $c^{\alpha}_{H_{(n-i)}P^{i-}}(0,t)$ is the bare i-anion and $c^{\alpha}_{[(H_{(n-i)}P)_jL_k]^{ji-}}(0,t)$ the ijk-complexed anion concentrations, $c^{\alpha}_{H^+}(0,t)$ the proton concentration, and $c^{\alpha}_{HO^-}(0,t)$ the hydroxide concentration at the interface ($x = 0$) at any time. $\Delta^{w}_{o}\phi^{o'}_{H_{(n-i)}P^{i-}}$, $\Delta^{w}_{o}\phi^{o'}_{[(H_{(n-i)}P)_jL_k]^{ji-}}$, $\Delta^{w}_{o}\phi^{o'}_{H^+}$, $\Delta^{w}_{o}\phi^{o'}_{HO^-}$ are the formal transfer potential of the i-anion, ijk-complexed anion, proton and hydroxide, respectively. F is the Faraday constant, T is the absolute temperature and R is the gas constant.

The technique considered in this work is cyclic voltammetry. A constant sweep potential value $|v| = |\frac{d\Delta\phi}{dt}|$ is applied to the system and the distribution of charged species is given by:

$$\frac{c^{o}_{H_{(n-i)}P^{i-}}(0,t)}{c^{w}_{H_{(n-i)}P^{i-}}(0,t)} = \exp\left[-\frac{iF}{RT}\left(\Delta^{w}_{o}\phi_{init} + vt - \Delta^{w}_{o}\phi^{o'}_{H_{(n-i)}P^{i-}}\right)\right] \tag{8}$$

Rearranging Eq. (8) according to Nicholson and Shain [40], Eq. (9) is obtained as follows:

$$\frac{c^{o}_{H_{(n-i)}P^{i-}}(0,t)}{c^{w}_{H_{(n-i)}P^{i-}}(0,t)} = \theta_{H_{(n-i)}P^{i-}}[S_\lambda(t)]^{-i} \tag{9}$$

where

$$\theta_{H_{(n-i)}P^{i-}} = \exp\left[-\frac{iF}{RT}\left(\Delta^{w}_{o}\phi_{init} - \Delta^{w}_{o}\phi^{o'}_{H_{(n-i)}P^{i-}}\right)\right] \tag{10}$$

and

$$S_\lambda(t) = \begin{cases} \exp(\sigma t) & 0 < t \leqslant \lambda \\ \exp[\sigma(2\lambda - t)] & t > \lambda \end{cases} \tag{11}$$

with $\sigma = \frac{Fv}{RT}$.

Similarly, the following equations are defined for the other charged species:

$$\frac{c^{o}_{[(H_{(n-i)}P)_jL_k]^{ji-}}(0,t)}{c^{w}_{[(H_{(n-i)}P)_jL_k]^{ji-}}(0,t)} = \theta_{[(H_{(n-i)}P)_jL_k]^{ji-}}[S_\lambda(t)]^{-ji} = \frac{\beta^{o}_{ijk}}{\beta^{w}_{ijk}}(K_{D,L})^{k}\left(\theta_{H_{(n-i)}P^{i-}}\right)^{j}[S_\lambda(t)]^{-ji} \tag{12}$$

$$\frac{c^{o}_{H^+}(0,t)}{c^{w}_{H^+}(0,t)} = \theta_{H^+}[S_\lambda(t)] \tag{13}$$

$$\frac{c^{o}_{HO^-}(0,t)}{c^{w}_{HO^-}(0,t)} = \theta_{HO^-}[S_\lambda(t)]^{-1} \tag{14}$$

The diffusion equations for the total anion (Eq. (18)), total ligand (Eq. (19)), and total charged species (Eq. (20)) concentrations are defined by Fick's laws according to Matsuda et al. [24] as follows:

$$\frac{\partial c^{\alpha}_{H_nPtot}}{\partial t} = D^{\alpha}\frac{\partial^2 c^{\alpha}_{H_nPtot}}{\partial x^2} \tag{15}$$

$$\frac{\partial c^{\alpha}_{Ltot}}{\partial t} = D^{\alpha}\frac{\partial^2 c^{\alpha}_{Ltot}}{\partial x^2} \tag{16}$$

$$\frac{\partial c^{\alpha}_{chargetot}}{\partial t} = D^{\alpha}\frac{\partial^2 c^{\alpha}_{chargetot}}{\partial x^2} \tag{17}$$

where the diffusion coefficients (D^{α}) are assumed to be the same for all species in each phase.

The total concentration of anions and neutral ligand are defined by the mass balance equations:

$$c^{\alpha}_{H_nPtot} = \sum_{i=0}^{n} c^{\alpha}_{H_{(n-i)}P^{i-}} + \sum_{k=1}^{l}\sum_{j=1}^{m}\sum_{i=1}^{n} jc^{\alpha}_{[(H_{(n-i)}P)_jL_k]^{ji-}} \tag{18}$$

$$c^{\alpha}_{Ltot} = c^{\alpha}_{L} + \sum_{k=1}^{l}\sum_{j=1}^{m}\sum_{i=1}^{n} kc^{\alpha}_{[(H_{(n-i)}P)_jL_k]^{ji-}} \tag{19}$$

and the total charged species concentration is defined as:

$$c^{\alpha}_{chargetot} = c^{\alpha}_{H^+} - \sum_{i=1}^{n} ic^{\alpha}_{H_{(n-i)}P^{i-}} - \sum_{k=1}^{l}\sum_{j=1}^{m}\sum_{i=1}^{n} jic^{\alpha}_{[(H_{(n-i)}P)_jL_k]^{ji-}} - c^{\alpha}_{HO^-} \tag{20}$$

Considering the boundary conditions, the fluxes of species across the interface are expressed by:

$$D^{w}\frac{\partial c^{w}_{H_nPtot}}{\partial x}\bigg|_{x=0} = D^{o}\frac{\partial c^{o}_{H_nPtot}}{\partial x}\bigg|_{x=0} = f_{H_nPtot}(t) \tag{21}$$

$$D^{w}\frac{\partial c^{w}_{Ltot}}{\partial x}\bigg|_{x=0} = D^{o}\frac{\partial c^{o}_{Ltot}}{\partial x}\bigg|_{x=0} = f_{Ltot}(t) \tag{22}$$

$$D^{w}\frac{\partial c^{w}_{chargetot}}{\partial x}\bigg|_{x=0} = D^{o}\frac{\partial c^{o}_{chargetot}}{\partial x}\bigg|_{x=0} = f_{chargetot}(t) \tag{23}$$

The total interfacial concentrations are expressed as a function of the convolution integrals using Laplace transforms:

$$c^{w}_{H_nPtot}(0,t) = c^{w,}_{H_nPtot} - \frac{1}{(\pi D^{w})^{\frac{1}{2}}}\int_0^t \frac{f_{H_nPtot}(\tau)d\tau}{(t-\tau)^{\frac{1}{2}}} \tag{24}$$

$$c^{o}_{H_nPtot}(0,t) = c^{o,}_{H_nPtot} + \frac{1}{(\pi D^{o})^{\frac{1}{2}}}\int_0^t \frac{f_{H_nPtot}(\tau)d\tau}{(t-\tau)^{\frac{1}{2}}} \tag{25}$$

$$c^{w}_{Ltot}(0,t) = c^{w,*}_{Ltot} - \frac{1}{(\pi D^{w})^{\frac{1}{2}}}\int_0^t \frac{f_{Ltot}(\tau)d\tau}{(t-\tau)^{\frac{1}{2}}} \tag{26}$$

$$c^{o}_{Ltot}(0,t) = c^{o,*}_{Ltot} + \frac{1}{(\pi D^{o})^{\frac{1}{2}}}\int_0^t \frac{f_{Ltot}(\tau)d\tau}{(t-\tau)^{\frac{1}{2}}} \tag{27}$$

$$c^{w}_{chargetot}(0,t) = c^{w,*}_{chargetot} - \frac{1}{(\pi D^{w})^{\frac{1}{2}}}\int_0^t \frac{f_{chargetot}(\tau)d\tau}{(t-\tau)^{\frac{1}{2}}} \tag{28}$$

$$c^{o}_{chargetot}(0,t) = c^{o,*}_{chargetot} + \frac{1}{(\pi D^{o})^{\frac{1}{2}}}\int_0^t \frac{f_{chargetot}(\tau)d\tau}{(t-\tau)^{\frac{1}{2}}} \tag{29}$$

$c^{\alpha,*}_{H_nPtot}$, $c^{\alpha,*}_{Ltot}$ and $c^{\alpha,*}_{chargetot}$ being the total anion concentration, the total ligand concentration and the total charged species concentration, respectively, in the phase at $t = 0$ and for all x values. The total initial concentration of all species in each phase can be calculated at $t = 0$ as a function of the total initial concentrations of anions ($c^{init}_{H_nP}$) and ligand (c^{init}_{L}) introduced into the system [37,38,41]. In the case of the total charged species concentration in the aqueous phase, it can be calculated as the sum of all the charged species considering the pH value as constant and equal to the initial pH value. This approximation is valid because at $t = 0$, the flux of current across the interface is zero and the system is in equilibrium.

The total concentration of every species in the system is obtained from Eqs. (24)–(29) by eliminating the convolution integrals:

$$c^{*}_{\mathrm{H}_n\mathrm{Ptot}} = c^{\mathrm{w}}_{\mathrm{H}_n\mathrm{Ptot}}(0,t) + \xi c^{\mathrm{o}}_{\mathrm{H}_n\mathrm{Ptot}}(0,t) \quad (30)$$

$$c^{*}_{\mathrm{Ltot}} = c^{\mathrm{w}}_{\mathrm{Ltot}}(0,t) + \xi c^{\mathrm{o}}_{\mathrm{Ltot}}(0,t) \quad (31)$$

$$c^{*}_{\mathrm{chargetot}} = c^{\mathrm{w}}_{\mathrm{chargetot}}(0,t) + \xi c^{\mathrm{o}}_{\mathrm{chargetot}}(0,t) \quad (32)$$

where $\xi = \left(\frac{D^{\mathrm{o}}}{D^{\mathrm{w}}}\right)^{\frac{1}{2}}$, $c^{*}_{\mathrm{H}_n\mathrm{Plot}}$, c^{*}_{Ltot} and $c^{*}_{\mathrm{chargetot}}$ are the total concentration of anion, ligand and charged species in the system, respectively.

It is possible to obtain all the concentration values at the interface at all simulation times using Eqs. (30)–(32).

In this study, a particular case is solved and analyzed. A system where 1:1, 1:2 and 2:1 complexes and three different anion species ($n = 3$) are present in both phases:

$$\begin{cases} c^{*}_{\mathrm{H_3Ptot}} = \sum_{i=0}^{3}\left(c^{\mathrm{w}}_{\mathrm{H}_{(3-i)}\mathrm{P}^{i-}}(0,t) + \xi c^{\mathrm{o}}_{\mathrm{H}_{(3-i)}\mathrm{P}^{i-}}(0,t)\right) \\ \quad + \sum_{k=1}^{2}\sum_{i=1}^{3}\left(c^{\mathrm{w}}_{[\mathrm{H}_{(3-i)}\mathrm{PL}_k]^{i-}}(0,t) + \xi c^{\mathrm{o}}_{[\mathrm{H}_{(3-i)}\mathrm{PL}_k]^{i-}}(0,t)\right) \\ \quad + \sum_{i=1}^{3} 2\left(c^{\mathrm{w}}_{[(\mathrm{H}_{(3-i)}\mathrm{P})_2\mathrm{L}]^{2i-}}(0,t) + \xi c^{\mathrm{o}}_{[(\mathrm{H}_{(3-i)}\mathrm{P})_2\mathrm{L}]^{2i-}}(0,t)\right) \\ c^{*}_{\mathrm{Ltot}} = c^{\mathrm{w}}_{\mathrm{L}}(0,t) + \xi c^{\mathrm{o}}_{\mathrm{L}}(0,t) + \sum_{k=1}^{2}\sum_{i=1}^{3} k\left(c^{\mathrm{w}}_{[\mathrm{H}_{(3-i)}\mathrm{PL}_k]^{i-}}(0,t) + \xi c^{\mathrm{o}}_{[\mathrm{H}_{(3-i)}\mathrm{PL}_k]^{i-}}(0,t)\right) \\ \quad + \sum_{i=1}^{3}\left(c^{\mathrm{w}}_{[(\mathrm{H}_{(3-i)}\mathrm{P})_2\mathrm{L}]^{2i-}}(0,t) + \xi c^{\mathrm{o}}_{[(\mathrm{H}_{(3-i)}\mathrm{P})_2\mathrm{L}]^{2i-}}(0,t)\right) \\ c^{*}_{\mathrm{chargetot}} = c^{\mathrm{w}}_{\mathrm{H}^+}(0,t) + \xi c^{\mathrm{o}}_{\mathrm{H}^+}(0,t) - \sum_{i=1}^{3} i\left(c^{\mathrm{w}}_{\mathrm{H}_{(3-i)}\mathrm{P}^{i-}}(0,t) + \xi c^{\mathrm{o}}_{\mathrm{H}_{(3-i)}\mathrm{P}^{i-}}(0,t)\right) \\ \quad - \sum_{k=1}^{2}\sum_{i=1}^{3} i\left(c^{\mathrm{w}}_{[\mathrm{H}_{(3-i)}\mathrm{PL}_k]^{i-}}(0,t) + \xi c^{\mathrm{o}}_{[\mathrm{H}_{(3-i)}\mathrm{PL}_k]^{i-}}(0,t)\right) \\ \quad - \sum_{i=1}^{3} 2i\left(c^{\mathrm{w}}_{[(\mathrm{H}_{(3-i)}\mathrm{P})_2\mathrm{L}]^{2i-}}(0,t) + \xi c^{\mathrm{o}}_{[(\mathrm{H}_{(3-i)}\mathrm{P})_2\mathrm{L}]^{2i-}}(0,t)\right) \\ \quad - c^{\mathrm{w}}_{\mathrm{HO}^-}(0,t) - \xi c^{\mathrm{o}}_{\mathrm{HO}^-}(0,t) \end{cases} \quad (33)$$

Rewriting Eq. (33) as a function of $c^{\mathrm{w}}_{\mathrm{L}}(0,t)$, $c^{\mathrm{w}}_{\mathrm{H}^+}(0,t)$ and $c^{\mathrm{w}}_{\mathrm{P}^{3-}}(0,t)$, the following equations are obtained:

$$\begin{cases} c^{*}_{\mathrm{H_3Ptot}} = c^{\mathrm{w}}_{\mathrm{P}^{3-}}(0,t)\sum_{i=1}^{4} A_i\left[c^{\mathrm{w}}_{\mathrm{H}^+}(0,t)\right]^{(4-i)} \\ \quad + c^{\mathrm{w}}_{\mathrm{P}^{3-}}(0,t)\sum_{k=1}^{2}\sum_{i=5}^{7} A_{i1k}\left(c^{\mathrm{w}}_{\mathrm{L}}(0,t)\right)^{k}\left[c^{\mathrm{w}}_{\mathrm{H}^+}(0,t)\right]^{(7-i)} \\ \quad + 2\left(c^{\mathrm{w}}_{\mathrm{P}^{3-}}(0,t)\right)^{2} c^{\mathrm{w}}_{\mathrm{L}}(0,t)\sum_{i=5}^{7} A_{i21}\left[c^{\mathrm{w}}_{\mathrm{H}^+}(0,t)\right]^{2(7-i)} \\ c^{*}_{\mathrm{Ltot}} = A_8 c^{\mathrm{w}}_{\mathrm{L}}(0,t) + c^{\mathrm{w}}_{\mathrm{P}^{3-}}(0,t)\sum_{k=1}^{2}\sum_{i=5}^{7} k A_{i1k}\left(c^{\mathrm{w}}_{\mathrm{L}}(0,t)\right)^{k}\left[c^{\mathrm{w}}_{\mathrm{H}^+}(0,t)\right]^{(7-i)} \\ \quad + \left(c^{\mathrm{w}}_{\mathrm{P}^{3-}}(0,t)\right)^{2} c^{\mathrm{w}}_{\mathrm{L}}(0,t)\sum_{i=5}^{7} A_{i21}\left[c^{\mathrm{w}}_{\mathrm{H}^+}(0,t)\right]^{2(7-i)} \\ c^{*}_{\mathrm{chargetot}} = A_9 c^{\mathrm{w}}_{\mathrm{H}^+}(0,t) - c^{\mathrm{w}}_{\mathrm{P}^{3-}}(0,t)\sum_{i=2}^{4}(i-1)A_i\left[c^{\mathrm{w}}_{\mathrm{H}^+}(0,t)\right]^{(4-i)} \\ \quad - c^{\mathrm{w}}_{\mathrm{P}^{3-}}(0,t)\sum_{k=1}^{2}\sum_{i=5}^{7}(i-4)A_{i1k}\left(c^{\mathrm{w}}_{\mathrm{L}}(0,t)\right)^{k}\left[c^{\mathrm{w}}_{\mathrm{H}^+}(0,t)\right]^{(7-i)} \\ \quad - 2\left(c^{\mathrm{w}}_{\mathrm{P}^{3-}}(0,t)\right)^{2} c^{\mathrm{w}}_{\mathrm{L}}(0,t)\sum_{i=5}^{7}(i-4)A_{i21}\left[c^{\mathrm{w}}_{\mathrm{H}^+}(0,t)\right]^{2(7-i)} \\ \quad - \frac{A_{10}}{c^{\mathrm{w}}_{\mathrm{H}^+}(0,t)} \end{cases} \quad (34)$$

where

$$A_1 = \left(1 + \xi K_{\mathrm{D,H_3P}}\right)\left(K^{\mathrm{w}}_{\mathrm{a},1}K^{\mathrm{w}}_{\mathrm{a},2}K^{\mathrm{w}}_{\mathrm{a},3}\right)^{-1} \quad (35)$$

$$A_2 = \left\{1 + \xi\theta_{\mathrm{H_2P^-}}\left[S_\lambda(t)\right]^{-1}\right\}\left(K^{\mathrm{w}}_{\mathrm{a},2}K^{\mathrm{w}}_{\mathrm{a},3}\right)^{-1} \quad (36)$$

$$A_3 = \left\{1 + \xi\theta_{\mathrm{HP^{2-}}}\left[S_\lambda(t)\right]^{-2}\right\}\left(K^{\mathrm{w}}_{\mathrm{a},3}\right)^{-1} \quad (37)$$

$$A_4 = \left\{1 + \xi\theta_{\mathrm{P^{3-}}}\left[S_\lambda(t)\right]^{-3}\right\} \quad (38)$$

$$A_{5jk} = \left\{\beta^{\mathrm{w}}_{1jk} + \xi\beta^{\mathrm{o}}_{1jk}\left(K_{D,\mathrm{L}}\right)^{k}\left(\theta_{\mathrm{H_2P^-}}\right)^{j}\left[S_\lambda(t)\right]^{-j}\right\}\left(K^{\mathrm{w}}_{\mathrm{a},2}K^{\mathrm{w}}_{\mathrm{a},3}\right)^{-j} \quad (39)$$

$$A_{6jk} = \left\{\beta^{\mathrm{w}}_{2jk} + \xi\beta^{\mathrm{o}}_{2jk}\left(K_{D,\mathrm{L}}\right)^{k}\left(\theta_{\mathrm{HP^{2-}}}\right)^{j}\left[S_\lambda(t)\right]^{-2j}\right\}\left(K^{\mathrm{w}}_{\mathrm{a},3}\right)^{-j} \quad (40)$$

$$A_{7jk} = \left\{\beta^{\mathrm{w}}_{3jk} + \xi\beta^{\mathrm{o}}_{3jk}\left(K_{D,\mathrm{L}}\right)^{k}\left(\theta_{\mathrm{P^{3-}}}\right)^{j}\left[S_\lambda(t)\right]^{-3j}\right\} \quad (41)$$

$$A_8 = 1 + \xi K_{\mathrm{D,L}} \quad (42)$$

$$A_9 = 1 + \xi\theta_{\mathrm{H^+}}\left[S_\lambda(t)\right] \quad (43)$$

$$A_{10} = K_{\mathrm{w}}\left\{1 + \xi\theta_{\mathrm{HO^-}}\left[S_\lambda(t)\right]^{-1}\right\} \quad (44)$$

In order to know the concentrations of anion, ligand and proton is necessary to solve Eq. (34). The method used for solving this equation is a modification of the Powell hybrid method (HYBRD and HYBRDJ included in the MINPACK libraries) [42–44].

By numeric integration of the convolution integrals, according to Nicholson and Shain [40]:

$$\int_0^t \frac{f_{\mathrm{chargetot}}(\tau)\,d\tau}{(t-\tau)^{\frac{1}{2}}} = -(\pi D^{w})^{\frac{1}{2}}\left[c^{\mathrm{o},*}_{\mathrm{chargetot}} - c^{\mathrm{o}}_{\mathrm{chargetot}}(0,t)\right] \quad (45)$$

it is possible to know the total current of the system:

$$I_{\mathrm{chargetot}}(t) = FAf_{\mathrm{chargetot}}(t) \quad (46)$$

where A is the interfacial area.

In this work, three different models are compared [37,38]:

(A) Unbuffered aqueous solutions with water autoprotolysis according to the generalized Eq. (34). Model herein referred to as UBASA model.
(B) Unbuffered aqueous solutions without water autoprotolysis according to the generalized Eq. (34), considering that $A_{10} = 0$. Model herein referred to as UBAS model.
(C) Buffered aqueous solutions with a constant $c^{\mathrm{w}}_{\mathrm{H^+}}(0,t)$ value in the generalized Eq. (34) during all the sweep scan potential (according to the model's suppositions (d) and (j)). Model herein referred to as BASA model.

2. Results and discussion

For all simulations, the fixed parameters are the following: T = 298.15 K, $\xi = 1.12$ (water|1,2-DCE interface), v = 0.050 V s^{-1}, $D^{\mathrm{w}} = 1.0 \times 10^{-5}$ cm^2 s^{-1} and A = 1.0 cm^2. A hydrophobic ligand or ionophore is considered, with $\log(K_{\mathrm{D,L}}) = 2.00$.

In all the cases, the initial potential will be taken as positive, i.e., the voltammetric scans will always start from the positive side of the potential window. By convention, the transfer of a negative (positive) charge from the aqueous (organic) phase to the organic (aqueous) phase will produce a net negative (positive) current.

Since the ratio between the initial concentrations of anion and ligand is not a reduced variable, two different behaviours are observed depending on which is varied. The initial concentration ratios between ligand and anion have been obtained at constant anion concentration ($c^{\mathrm{init}}_{\mathrm{H_3P}} = 1.00$ mM) or at constant ligand concentration ($c^{\mathrm{init}}_{\mathrm{L}} = 1.00$ mM).

2.1. Interfacial complexation of H_2PL^-

2.1.1. Effect of water hydrolysis on anion transfer processes

In this section, we analyze and compare the effect of water autoprotolysis in the BASA, UBASA and UBAS models. Fig. 1a shows the voltammograms obtained with the different models for the transfer of H_2P^- assisted by L present in the organic phase. The initial pH in each case is such that the H_2P^- and HP^{2-} concentrations in the aqueous solution are comparable.

The voltammograms obtained for unbuffered aqueous solutions show two clearly defined transfer processes. The peak process at high potential values corresponds to the facilitated transfer of H_2P^- formed in the aqueous phase, and the other process to the facilitated transfer of H_2P^- *via* water hydrolysis (UBASA model) or with formation of P^{3-} (UBAS model). In the case of the BASA model, only one process is observed in the potential window. This process is associated with the facilitated transfer of H_2P^- present in the aqueous phase or formed from the reaction between H^+ and HP^{2-}.

It is important to highlight that the peak-to-peak potential difference of the second process, $\Delta\left(\Delta_o^w\phi_{peak}\right)$, is higher than that expected from a charge equal to −1. The $\Delta\left(\Delta_o^w\phi_{peak}\right)$ values for this process are 69 (UBASA model) and 83 mV (UBAS model). In these models, it is assumed that the transfer of all species through the interface is reversible and diffusion-controlled (supposition (e) in the theoretical section); therefore, $\Delta\left(\Delta_o^w\phi_{peak}\right)$ values are determined by a mixed diffusion regime and by previous coupled chemical reactions [26,27,31,32,37,38].

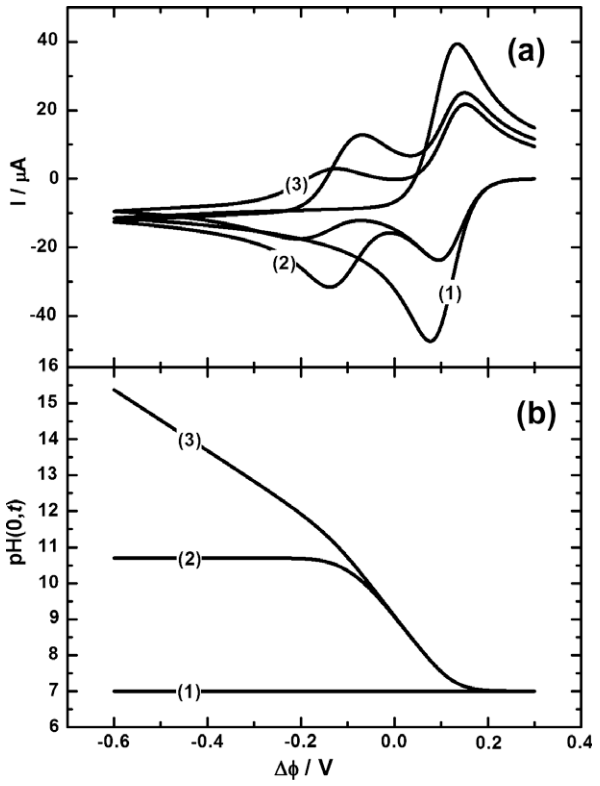

Fig. 1. Simulation results for the interfacial complexation of H_2PL^-. (a) Comparative voltammograms and (b) evolution of the $pH(0,t)$ as a function of the applied potential obtained for the BASA (1), UBASA (2) and UBAS (3) models. pH 7.00. $pK_{a,1}^w = 2.00$, $pK_{a,2}^w = 7.00$, $pK_{a,3}^w = 12.0$, $\beta_{ijk}^{\alpha} = 0.00$ except for $\log(\beta_{111}^o) = 20.0$, p$K_w = 14.0$, $\Delta_o^w\phi_{H^+}^{o'} = 0.55$V, $\Delta_o^w\phi_{HO^-}^{o'} = -1.00$V, $\Delta_o^w\phi_{H_2P^-}^{o'} = -1.00$V, $\Delta_o^w\phi_{HP^{2-}}^{o'} = -1.20$ V, $\Delta_o^w\phi_{P^{3-}}^{o'} = -1.40$V, $\log(K_{D,L}) = 2.00$, $\log(K_{D,H_3P}) = -5.00$, $c_{H_3P}^{init} = 1.00$ mM and $c_L^{init} = 100.0$ mM.

In Fig. 1b we can observe the variation of $pH(0,t)$ as a function of the applied potential. In the UBAS model, the interfacial proton concentration decreases indefinitely ($pH(0,t) > 14$) since it is consumed by the H_2PL^- formation in the organic phase. This result proves that the UBAS model does not represent a real system, in which the water molecules would buffer the interface as the H^+ ions are consumed. The importance of the inclusion of water autoprotolysis in the model is evidenced by the occurrence of two transfer processes with the real variation of the interfacial pH (see line 2, Fig. 1b).

According to the previous results, the global reactions for the facilitated transfer of H_2P^- can be postulated as following:

$$H_2P^-(w) + L(o) \rightleftharpoons H_2PL^-(o) \quad (R1)$$

in all the models analyzed; and for BASA model:

$$HP^{2-}(w) + H^+(w) + L(o) \rightleftharpoons H_2PL^-(o) \quad (R2)$$

or UBASA model:

$$HP^{2-}(w) + H_2O + L(o) \rightleftharpoons H_2PL^-(o) + HO^-(w) \quad (R3)$$

or

$$2HP^{2-}(w) + L(o) \rightleftharpoons H_2PL^-(o) + P^{3-}(w) \quad (R4)$$

when the anion concentration is high enough so that protons are provided by an acid weaker than water (HP^{2-}). Reactions (R1) and (R2) occur at the same applied potential, whereas reactions (R3) and (R4) involve higher energy transfers.

2.1.2. Effect of pH

In this section, we will analyze the variation of the peak transfer potential for the forward scan, $\Delta_o^w\phi_{peak}$, and the peak-to-peak potential difference, $\Delta\left(\Delta_o^w\phi_{peak}\right)$, as a function of pH. Fig. 2 shows the variation of $\Delta_o^w\phi_{peak}$ and $\Delta_o^w\phi_{peak}$ for three different concentration ratios between the ligand and the anion. When buffered aqueous solutions are considered (BASA model), the peak potential shows a linear relationship with a slope of −59 mV/decade, in the pH range between 8 and 11. Within this pH range, HP^{2-} is the predominant species in the aqueous phase. Moreover, $\Delta_o^w\phi_{peak}$ reaches a constant value in the pH range of 3–7. The transfer process is further facilitated in the pH range between 3 and 7 and has a maximum value when the ligand or the anion is in excess ($c_L^{init} \gg c_{H_3P}^{init}$ or $c_L^{init} \ll c_{H_3P}^{init}$). In the UBASA model, the three concentration ratios analyzed present a pH range where the current–potential profiles show two well-defined charge transfer processes. The transfer process at more positive potential is associated with reaction (R1), and the second process occurs via water autoprotolysis (reaction (R3)). Outside the pH range, where two different charge transfer processes take place, the potential transfer values obtained with BASA and UBASA models are the same.

It is remarkable that the dependence change of the potential transfer with pH depends only on the pK_{a,H_nP}^w values of the H_3P species. This behaviour is due to the high hydrophilicity of H_3P and the anionic species. The points where $pH = pK_{a,H_nP}^w$ are marked in Fig. 2 are intended to facilitate the comparison between the acid–base equilibria and the potential transfer behaviour.

Fig. 2d shows the $\Delta\left(\Delta_o^w\phi_{peak}\right)$ for the three concentration ratios between the ligand and the anion. $\Delta\left(\Delta_o^w\phi_{peak}\right)$ values obtained with the BASA model are 59 mV for $c_L^{init} \gg c_{H_3P}^{init}$ or $c_L^{init} \ll c_{H_3P}^{init}$ and 84 mV for $c_L^{init} = c_{H_3P}^{init}$. The latter $\Delta\left(\Delta_o^w\phi_{peak}\right)$ value is a consequence of mixed diffusion regime of the neutral ligand in organic phase and the anions or H_3P, depending on the pH value, in aqueous phase [27,32,37,38]. For both model, when $pH < pK_{H_2P^-}^w$ and ligand or anion in excess, the potential difference is equal to 59 mV. For UBASA model, when $pK_{H_2P^-}^w < pH < pK_{HP^{2-}}^w$, $\Delta\left(\Delta_o^w\phi_{peak}\right)$ reaches a maximum value of 90 mV. In the case of $c_L^{init} = c_{H_3P}^{init}$, when

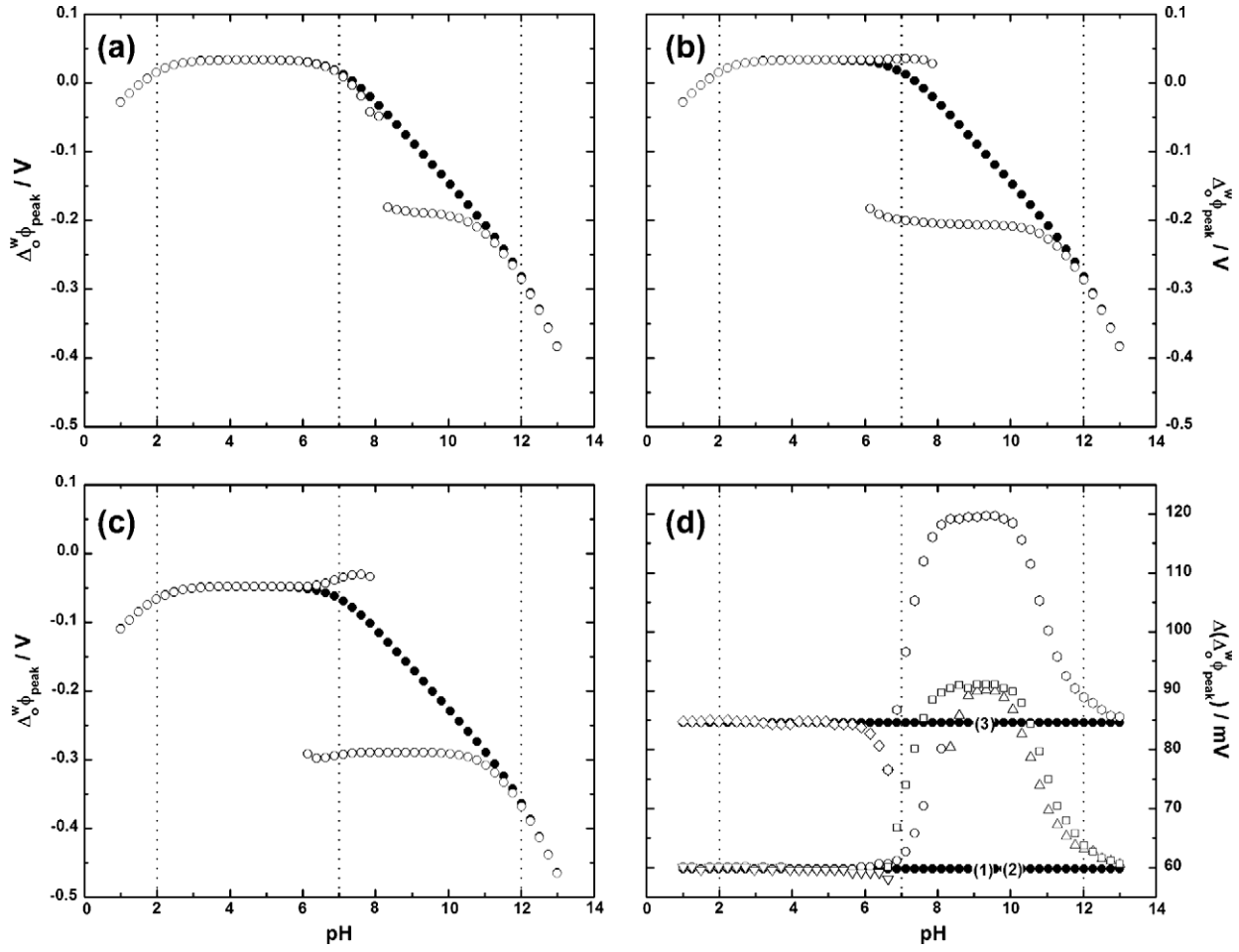

Fig. 2. Simulation results for the interfacial complexation of H_2PL^-. Variation of the peak transfer potential for the forward scan as a function of pH. Simulations obtained by BASA (filled circle) and UBASA (open circle) models and for different experimental conditions: (a) $c_{H_3P}^{init} \gg c_L^{init}$, (b) $c_{H_3P}^{init} \ll c_L^{init}$ and (c) $c_{H_3P}^{init} = c_L^{init}$. Variation of the peak-to-peak potential difference as a function of pH (d). Simulations obtained by BASA model (filled circle): (1) $c_{H_3P}^{init} \gg c_L^{init}$, (2) $c_{H_3P}^{init} \ll c_L^{init}$ and (3) $c_{H_3P}^{init} = c_L^{init}$, and UBASA model: (open circle and open triangle up) $c_{H_3P}^{init} \gg c_L^{init}$ (open triangle down and open square) $c_{H_3P}^{init} \ll c_L^{init}$ and (open diamond and open hexagon) $c_{H_3P}^{init} = c_L^{init}$. Simulated results correspond to the first charge transfer process (open circle, open triangle down and open diamond) and the second charge transfer process (open triangle up, open square and open hexagon). Panel (a): $c_{H_3P}^{init} = 1.00$ mM and $c_L^{init} = 100.0$ mM; panel (b) $c_{H_3P}^{init} = 100.0$ mM and $c_L^{init} = 1.00$ mM and (c) $c_{H_3P}^{init} = c_L^{init} = 1.00$ mM. Other parameters are the same as those in Fig. 1.

$pH < pK_{H_2P^-}^w$, the potential difference is equal to 84 mV. For $pK_{H_2P^-}^w < pH < pK_{HP^{2-}}^w$, the potential difference reaches a maximum value of 120 mV. In general, when $pK_{H_2P^-}^w < pH < pK_{HP^{2-}}^w$ and for all concentration ratios, the charge transfer process is controlled by mixed diffusion regime, defined by L in the organic phase and HP^{2-} in the aqueous phase, and coupled chemical reactions [37,38].

2.1.3. Effect of the initial concentration of the ligand and anion species

This section is devoted to analyze the effect of the initial concentration of ligand and anion on the charge transfer processes. To increase the effect of coupled chemical reactions, the analysis is performed at pH = 9.5, where HP^{2-} is the predominant species in the aqueous phase. In this experimental condition, facilitated anion transfer occurs according to reaction (R2) for BASA model or reactions (R3) and (R4) for UBASA model.

Fig. 3 shows the peak potential for the forward scan and the peak-to-peak potential difference as a function of the concentration ratios between ligand and anion. These amounts have been obtained by fixing the concentration of anion or ligand. When the BASA model is considered, both the peak potential and the peak-to-peak potential difference present the same behaviour in both conditions. When $c_L^{init} \gg c_{H_3P}^{init}$(fixed) (or $c_{H_3P}^{init} \gg c_L^{init}$(fixed)), the $\Delta_o^w\phi_{peak}$ shifts by 59 mV (−59 mV) per decade of concentration ratio. Conversely, when $c_L^{init} \ll c_{H_3P}^{init}$(fixed) (or $c_{H_3P}^{init} \ll c_L^{init}$(fixed)), the potential peak remains constant. For concentration ratios close to one, the peak potential corresponds to that of mixed diffusion regime [26,27,31,32,37,38]. For the UBASA model, the limiting behaviours are equivalent to the BASA model, but for concentration ratios close to one, $\Delta_o^w\phi_{peak}$ also depends on the chemical reactions coupled to charge transfer process [37,38].

The effect of mixed diffusion regime and chemical reactions coupled to charge transfer process is corroborated by the variation of the peak-to-peak potential difference shown in Fig. 3b. In this figure, typical current–potential profiles for different concentration ratios for both models are found. The $\Delta(\Delta_o^w\phi_{peak})$ values for BASA model correspond to those reported previously in the literature for cation transfer assisted by neutral ligands [27,28,32,38] and protonated species transfer [37,38]. It is important to highlight that the peak-to-peak potential difference, in the case of the UBASA model, is higher than that expected from a charge equal to −1. $\Delta(\Delta_o^w\phi_{peak})$ reaches a maximum value of 120 mV and for $c_L^{init} \gg c_{H_3P}^{init}$(fixed), $\Delta(\Delta_o^w\phi_{peak})$ remains constant with a value equal to 89 mV. Furthermore, when the concentration of ligand is fixed at 1.0 mM, the limiting behaviours of the potential value are equal to those obtained with the BASA model (59 mV). Moreover, $\Delta(\Delta_o^w\phi_{peak})$ present an interesting behaviour for $\log(c_L^{init}/c_{H_3P}^{init}) \cong$

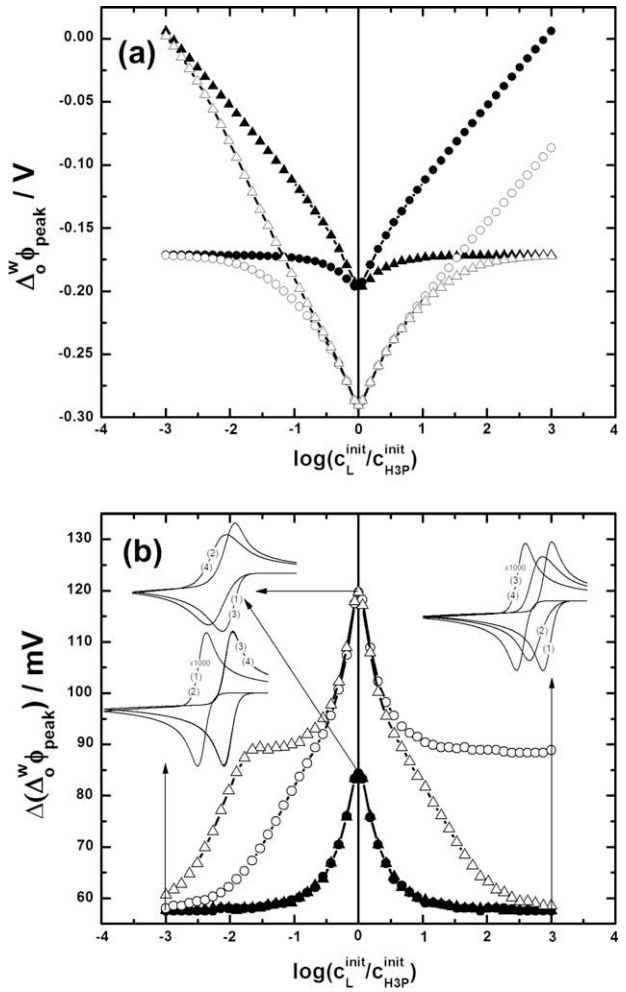

Fig. 3. Simulation results for the interfacial complexation of H_2PL^-. Variation of the peak transfer potential for the forward scan (a) and peak-to-peak potential difference (b) as a function of $\log\left(c_L^{init}/c_{H_3P}^{init}\right)$. Simulations obtained for a constant anion concentration $\left(c_{H_3P}^{init} = 1.00\ \text{mM}\right)$ ((filled circle) BASA model and (open circle) UBASA model) and a constant ligand concentration $(c_L^{init} = 1.00\ \text{mM})$ ((filled triangle up) BASA model and (open triangle up) UBASA model). Panel (b): Voltammogram obtained for a constant anion concentration $\left(c_{H_3P}^{init} = 1.00\ \text{mM}\right)$ ((1) BASA model and (2) UBASA model) and a constant ligand concentration $(c_L^{init} = 1.00\ \text{mM})$ ((3) BASA model and (4) UBASA model). pH 9.50. Other parameters are the same as those in Fig. 1.

-2.0. For $-2.0 < \log(c_L^{init}/c_{H_3P}^{init}) < -0.5$, the peak-to-peak potential difference is equal to 89 mV and the charge transfer process occurs via reaction (R3). For $\log(c_L^{init}/c_{H_3P}^{init}) < -2.0$, reaction (R4) with the formation of P^{3-} species at the interface prevails (see Section 2.1.1).

2.2. Interfacial complexation of $H_2PL_2^-$

2.2.1. Effect of pH

As in Section 2.1.2, we will here examine the variation of the peak transfer potential, $\Delta_o^w\phi_{peak}$, for the forward scan and the peak-to-peak potential difference, $\Delta(\Delta_o^w\phi_{peak})$, with pH. To increase the effect of mixed diffusion regime, the analysis is performed for $c_L^{init} = 2c_{H_3P}^{init}$. Fig. 4 compares the variation of $\Delta_o^w\phi_{peak}$ and $\Delta(\Delta_o^w\phi_{peak})$ for BASA and UBASA models. The general behaviour of the peak potential is equivalent to that found in Fig. 2c. When buffered aqueous solutions are considered (BASA model), the peak potential shows a linear relationship of pH with a slope of -59 mV/decade, in the pH range between 8 and 11. In addition, $\Delta_o^w\phi_{peak}$ reaches a constant value in the pH range between 3 and 7. The UBASA model displays a pH range in which the current–potential profiles show two well-defined charge transfer processes. The transfer process at more positive potential is associated with reaction (R5) and the other process occurs via water autoprotolysis (reaction (R7)). Outside the pH range where two different charge transfer processes take place, the potential transfer values obtained with BASA and UBASA models are the same.

Accordingly, the overall reactions for the facilitated transfer of H_2P^- can be postulated as following:

$$H_2P^-(w) + 2L(o) \rightleftharpoons H_2PL_2^-(o) \quad (R5)$$

for both models, and, for BASA model:

$$HP^{2-}(w) + H^+(w) + 2L(o) \rightleftharpoons H_2PL_2^-(o) \quad (R6)$$

or for UBASA model:

$$HP^{2-}(w) + H_2O + 2L(o) \rightleftharpoons H_2PL_2^-(o) + HO^-(w) \quad (R7)$$

or

$$2HP^{2-}(w) + 2L(o) \rightleftharpoons H_2PL_2^-(o) + P^{3-}(w) \quad (R8)$$

depending on the initial concentration of HP^{2-}.

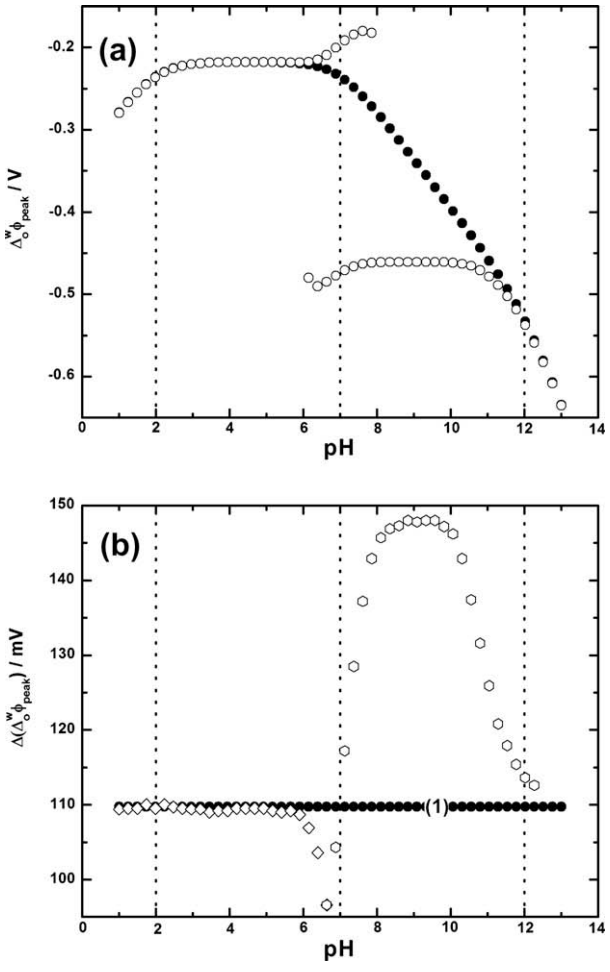

Fig. 4. Simulation results for the interfacial complexation of H_2PL_2. Variation of the peak transfer potential for the forward scan as a function of pH (a). Simulations obtained for BASA (filled circle) and UBASA (open circle) models for $c_L^{init} = 2c_{H_3P}^{init}$. Variation of the peak-to-peak potential difference as a function of pH (b). Simulations obtained by BASA model (filled circle) and UBASA model (open diamond and open hexagon). Simulated results correspond to the first charge transfer process (open circle) and the second charge transfer process (open hexagon). $\beta_{ijk}^z = 0.00$ except for $\log(\beta_{112}^o) = 20.0$ and $c_L^{init} = 2c_{H_3P}^{init} = 2.00$ mM. Other parameters are the same as those in Fig. 1.

Reactions (R5) and (R6) occur at the same applied potential, whereas reactions (R7) and (R8) involve higher energy transfers than reactions (R5) and (R6).

The $\Delta(\Delta_o^w\phi_{peak})$ value obtained with the BASA model is 109.9 mV for $c_L^{init} = 2c_{H_3P}^{init}$ (see Fig. 4b). This $\Delta(\Delta_o^w\phi_{peak})$ value is a consequence of mixed diffusion regime [26,27,31,32,37,38]. For the UBASA model, when $pH < pK_{H_2P^-}^w$ the $\Delta(\Delta_o^w\phi_{peak})$ is equal to 109.9 mV and for $pK_{H_2P^-}^w < pH < pK_{HP^{2-}}^w$, $\Delta(\Delta_o^w\phi_{peak})$ reaches a maximum value of 149 mV. In this pH range, the charge transfer process is controlled by mixed diffusion regime and coupled chemical reactions [37,38].

2.2.2. Effect of the initial concentration of the ligand and anion species

To increase the effect of coupled chemical reactions, the analysis is performed at pH 9.5, where HP^{2-} is the predominant species in the aqueous phase. In this experimental condition, facilitated anion transfer occurs according to reaction (R6) for BASA model and reactions (R7) or (R8) for UBASA model.

Fig. 5 shows the peak potential for the forward scan and the peak-to-peak potential difference as a function of the concentration ratios between ligand and anion. When the BASA model is considered, the peak potential as the peak-to-peak potential difference exhibited the same behaviour in both conditions. When $c_L^{init} \gg c_{H_3P}^{init}$(fixed) (or $c_{H_3P}^{init} \gg c_L^{init}$(fixed)), $\Delta_o^w\phi_{peak}$ shifts by 118 mV (−59 mV) per decade of concentration ratio. On the other hand, for $c_L^{init} \ll c_{H_3P}^{init}$(fixed), $\Delta_o^w\phi_{peak}$ shifts by −59 mV per decade of concentration ratio. Conversely, when $c_{H_3P}^{init} \ll c_L^{init}$(fixed), the potential peak remains constant. For concentration ratios close to log(2), the peak potential is defined by a mixed diffusion regime [26,27,31,32,37,38]. For the UBASA model the limiting behaviours are equivalent to the BASA model, but for concentration ratios close to one, $\Delta_o^w\phi_{peak}$ also depends on the chemical reactions coupled to charge transfer process [37,38].

Fig. 5b shows the peak-to-peak potential difference as a function of the concentration ratios between ligand and anion. The figure shows typical current–potential profiles for different concentration ratios from both models. The $\Delta(\Delta_o^w\phi_{peak})$ values for BASA model correspond to those reported previously in the literature for the formation of complexes with cations [27]. It is important to note that the peak-to-peak potential difference, in the case of the UBASA model, is higher than that expected from a charge equal to −1 and a stoichiometry 1:2. $\Delta(\Delta_o^w\phi_{peak})$ reaches a maximum value of 149 mV and for $c_L^{init} \gg c_{H_3P}^{init}$, $\Delta(\Delta_o^w\phi_{peak})$ remains constant with a value equal to 88.5 mV. Furthermore, when the concentration of ligand is fixed at 1.0 mM, the limiting behaviours of the potential peaks are equal to those obtained with the BASA model (59 mV for $c_{H_3P}^{init} \ll c_L^{init}$(fixed) and 85.5 mV for $c_{H_3P}^{init} \gg c_L^{init}$(fixed)). Moreover, $\Delta(\Delta_o^w\phi_{peak})$ present an interesting behaviour for $\log(c_L^{init}/c_{H_3P}^{init}) \cong -1.0$. For $-1.0 < \log(c_L^{init}/c_{H_3P}^{init}) < -0.5$, the peak-to-peak potential difference is equal to 120 mV and the charge transfer process occurs via reaction (R7). For $\log(c_L^{init}/c_{H_3P}^{init}) < -1.0$, reaction (R8) prevails, and P^{3-} is formed at the interface.

2.3. Interfacial complexation of $(H_2P)_2L^{2-}$

2.3.1. Effect of pH

In this section we examine the variation of $\Delta_o^w\phi_{peak}$ for the forward scan and $\Delta(\Delta_o^w\phi_{peak})$ as a function of pH for the formation of complexes with 2:1 anion-to-ligand stoichiometry. To increase the effect of mixed diffusion regime, the analysis is carried out for $2c_L^{init} = c_{H_3P}^{init}$. Fig. 6 compares the variation of $\Delta_o^w\phi_{peak}$ and $\Delta(\Delta_o^w\phi_{peak})$ for BASA and UBASA models. The general behaviour of the peak potential is equivalent to that found in Fig. 2c. When buffered aqueous solutions are considered (BASA model), the peak potential shows a linear relationship of pH with a slope of −59 mV/

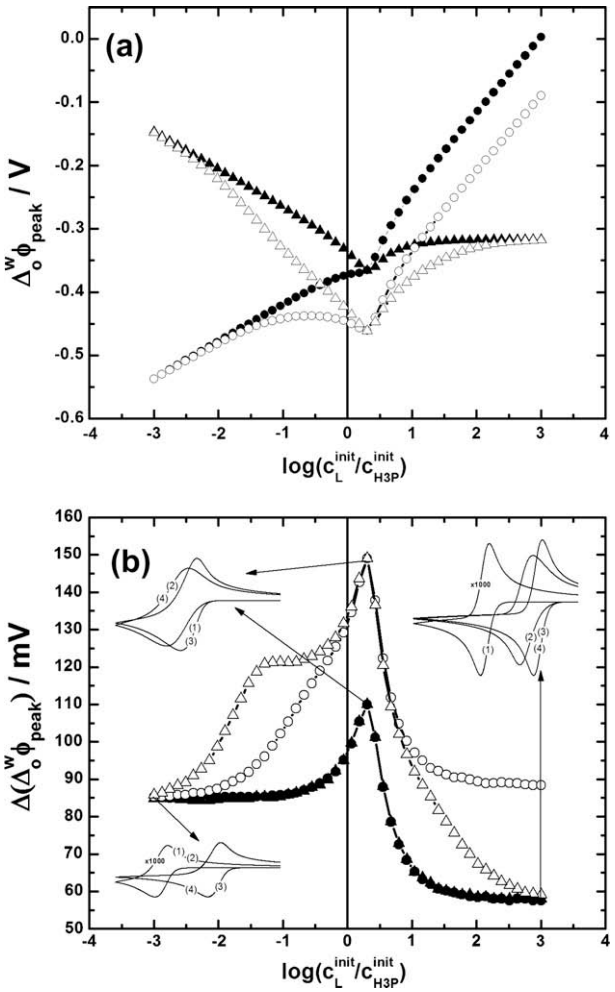

Fig. 5. Simulation results for the interfacial complexation of H_2PL_2. Variation of the peak transfer potential for the forward scan (a) and peak-to-peak potential difference (b) as a function of $\log(c_L^{init}/c_{H_3P}^{init})$. Simulations obtained by a constant anion concentration ($c_{H_3P}^{init} = 1.00$ mM) ((filled circle) BASA model and (open circle) UBASA model) and a constant ligand concentration ($c_L^{init} = 2.00$ mM) ((filled triangle up) BASA model and (open triangle up) UBASA model). Panel (b): Voltammogram obtained for a constant anion concentration ($c_{H_3P}^{init} = 1.00$ mM) ((1) BASA model and (2) UBASA model) and a constant ligand concentration ($c_L^{init} = 2.00$ mM) ((3) BASA model and (4) UBASA model). pH 9.50. Other parameters are the same as those in Fig. 4.

decade, in the pH range between 8 and 11. In addition, $\Delta_o^w\phi_{peak}$ reaches a constant value in the pH range between 3 and 7. The UBASA model exhibits a pH range where the current–potential profiles show two well-defined charge transfer processes. The transfer process at more positive potential is associated with reaction (R9) and the second process takes place via water autoprotolysis (reaction (R11)). Outside the pH range, where two different charge transfer processes occur, the potential transfer values obtained with BASA and UBASA models are the same.

Therefore, the overall reactions for the facilitated transfer of H_2P^- can be postulated as follows:

$$2H_2P^-(w) + L(o) \rightleftharpoons (H_2P)_2L^{2-}(o) \quad (R9)$$

for both models;

$$2HP^{2-}(w) + 2H^+(w) + L(o) \rightleftharpoons (H_2P)_2L^{2-}(o) \quad (R10)$$

for BASA model; or:

$$2HP^{2-}(w) + 2H_2O + L(o) \rightleftharpoons (H_2P)_2L^{2-}(o) + 2HO^-(w) \quad (R11)$$

or

$$4HP^{2-}(w) + L(o) \rightleftharpoons (H_2P)_2L^{2-}(o) + 2P^{3-}(w) \quad (R12)$$

for UBASA model.

The last reaction occurs when the anion concentration is high enough so that protons are provided by an acid weaker than water (HP^{2-}).

Reactions (R9) and (R10) occur at the same applied potential, whereas reactions (R11) and (R12) involve higher energy transfers than reactions (R9) and (R10).

$\Delta(\Delta_o^w\phi_{peak})$ values (see Fig. 6b) obtained with the BASA model is 54.8 mV for $2c_L^{init} = c_{H_3P}^{init}$. This $\Delta(\Delta_o^w\phi_{peak})$ value is a consequence of the mixed diffusion regime [26,27,31,32,37,38]. For the UBASA model, when $pH < pK_{H_2P^-}^w$ the $\Delta(\Delta_o^w\phi_{peak})$ is equal to 54.8 mV and for $pK_{H_2P^-}^w < pH < pK_{HP^{2-}}^w$, $\Delta(\Delta_o^w\phi_{peak})$ reaches a maximum value of 94.1 mV. In this pH range, the charge transfer process is controlled by mixed diffusion regime and coupled chemical reactions [37,38].

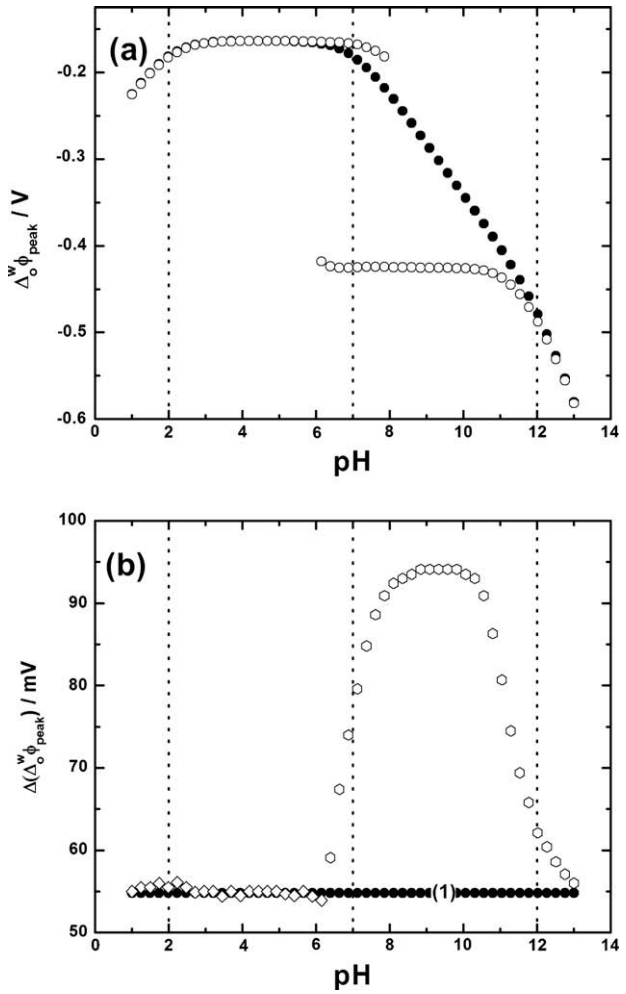

Fig. 6. Simulation results for the interfacial complexation of $(H_2P)_2L^-$. Variation of the peak transfer potential for the forward scan as a function of pH (a). Simulations obtained for BASA (filled circle) and UBASA (open circle) models for $c_{H_3P}^{init} = 2c_L^{init}$. Variation of the peak-to-peak potential difference as a function of pH (b). Simulations obtained by BASA model (filled circle) and UBASA model (open diamond and open hexagon). Simulated results correspond to the first charge transfer process (open circle) and the second charge transfer process (open hexagon). $\beta_{ijk}^{\infty} = 0.00$ except for $\log(\beta_{121}^{o}) = 35.0$ and $c_{H_3P}^{init} = 2c_L^{init} = 2.00$ mM. Other parameters are the same as those in Fig. 1.

2.3.2. Effect of the initial concentration of the ligand and anion species

In this section, we analyze the effect of the initial concentration of the ligand and the anion on the charge transfer processes for the formation of $(H_2P)_2L^{2-}$. To increase the effect of coupled chemical reactions, the analysis is performed at pH = 9.5 where HP^{2-} is the predominant species in the aqueous phase. In this experimental condition, facilitated anion transfer occurs according to reaction (R10), or reactions (R11) or (R12) for BASA or UBASA models, respectively.

Fig. 7 indicates the peak potential for the forward scan and the peak-to-peak potential difference as a function of the concentration ratios. For the BASA model, both, the peak potential and the peak-to-peak potential difference show the same behaviour in each experimental conditions ($c_{H_3P}^{init}$(fixed) or c_L^{init}(fixed)). When $c_L^{init} \gg c_{H_3P}^{init}$(fixed) (or $c_{H_3P}^{init} \gg c_L^{init}$(fixed)), $\Delta_o^w\phi_{peak}$ shifts by 28.5 mV (−59 mV) per decade of concentration ratio, whereas for $c_L^{init} \ll c_{H_3P}^{init}$(fixed), the potential peak remains constant. Conversely, when $c_{H_3P}^{init} \ll c_L^{init}$(fixed), $\Delta_o^w\phi_{peak}$ shifts by −59 mV per decade of concentration ratio. For concentration ratios close to $-\log(2)$, the peak potential is defined by a mixed diffusion regime [26,27,31,32,37,38].

Fig. 7b shows the peak-to-peak potential difference as a function of the concentration ratios between ligand and anion. It also shows typical current–potential profiles for different concentration ratios from both models. For BASA model, $\Delta(\Delta_o^w\phi_{peak})$ reaches a maximum value of 54.9 mV. $\Delta(\Delta_o^w\phi_{peak})$ remains constant with a value equal to 29.6 mV and 42.6 mV for $c_L^{init} \ll c_{H_3P}^{init}$(fixed) and $c_L^{init} \gg c_{H_3P}^{init}$(fixed), respectively. It should be noted that the peak-to-peak potential difference, in the case of the UBASA model, is higher than that expected from a charge equal to −2. $\Delta(\Delta_o^w\phi_{peak})$ reaches a maximum value of 94.6 mV and for $c_L^{init} \gg c_{H_3P}^{init}$(fixed), $\Delta(\Delta_o^w\phi_{peak})$ remains constant with a value equal to 79.8 mV.

Furthermore, when the concentration of ligand is fixed at 1.0 mM, the limiting behaviours of the potential are equal to those obtained with the BASA model (42.6 mV for $c_{H_3P}^{init} \ll c_L^{init}$(fixed) and ≅30 mV for $c_{H_3P}^{init} \gg c_L^{init}$(fixed)). Moreover, $\Delta(\Delta_o^w\phi_{peak})$ present an interesting behaviour for $\log(c_L^{init}/c_{H_3P}^{init}) \cong -2.0$. For $-2.0 < \log(c_L^{init}/c_{H_3P}^{init}) < -1.5$, the peak-to-peak potential difference is equal to 60 mV and the charge transfer process occurs via reaction (R11). For $\log(c_L^{init}/c_{H_3P}^{init}) < -2.0$, reaction (R12) prevails and P^{3-} is formed at the interface.

2.4. Analysis of the facilitated anion transfer for different anion-to-ligand stoichiometries

We first perform a comparative analysis of the effect of water autoprotolysis on the facilitated anion transfer. To quantify this effect we define the change of the free energy transfer as follows:

$$\Delta\left(\Delta G_{tr}^{0',w\to o}\right) = \Delta G_{tr,\text{BASA model}}^{0',w\to o} - \Delta G_{tr,\text{UBASA model}}^{0',w\to o} \quad (47)$$

where, $\Delta G_{tr,\text{BASA model}}^{0',w\to o}$ and $\Delta G_{tr,\text{UBASA model}}^{0',w\to o}$ are the free energy transfers obtained for unbuffered and buffered aqueous solutions, respectively. The change in free energy quantifies the extra energy necessary for the breakdown of water molecules to produce the protons involved in the transfer of the anion. The BASA model provides the minimum energy required for the transfer and therefore the $\Delta(\Delta G_{tr}^{0',w\to o})$ is defined according to Eq. (47). Fig. 8 shows the variation of $\Delta(\Delta G_{tr}^{0',w\to o})$ as a function of the concentration ratios between the ligand and the anion for the systems analyzed in Figs. 3, 5 and 7

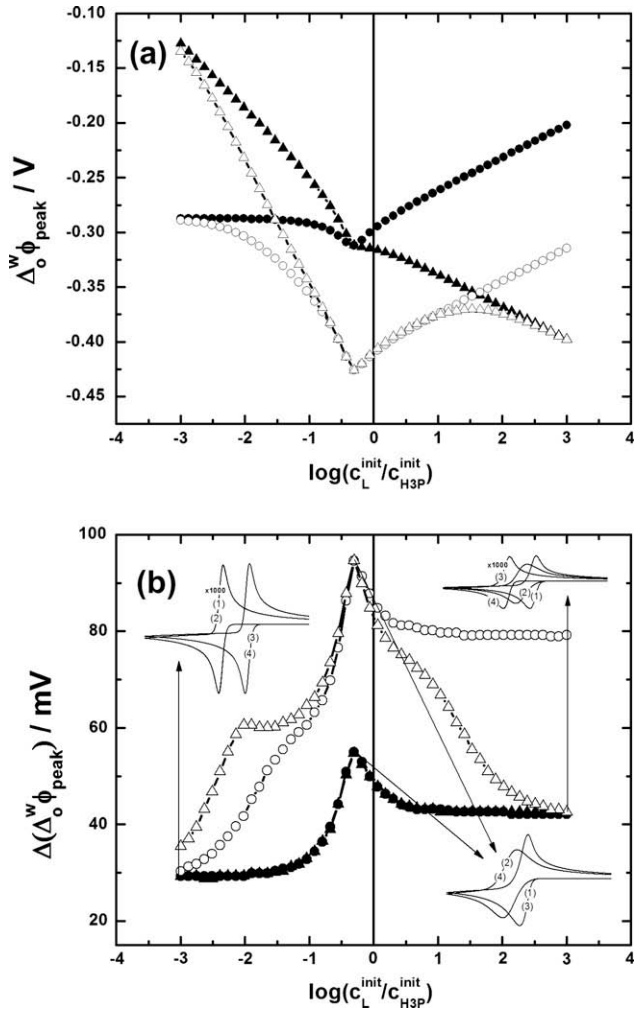

Fig. 7. Simulation results for the interfacial complexation of $(H_2P)_2L^-$. Variation of the peak transfer potential for the forward scan (a) and peak-to-peak potential difference (b) as a function of $\log\left(c_L^{init}/c_{H_3P}^{init}\right)$. Simulations obtained by a constant anion concentration $\left(c_{H_3P}^{init} = 2.00\ mM\right)$ ((filled circle) BASA model and (open circle) UBASA model) and a constant ligand concentration $(c_L^{init} = 1.00\ mM)$ ((filled triangle up) BASA model and (open triangle up) UBASA model). Panel (b): Voltammogram obtained for a constant anion concentration $\left(c_{H_3P}^{init} = 2.00\ mM\right)$ ((1) BASA model and (2) UBASA model) and a constant ligand concentration $(c_L^{init} = 1.00\ mM)$ ((3) BASA model and (4) UBASA model). pH 9.50. Other parameters are the same as those in Fig. 6.

(particularly where $c_{H_3P}^{init}$ is fixed). $\Delta\left(\Delta G_{tr}^{0',w\to o}\right)$ increases as the concentration ratio becomes more positive until reaching a constant value for all stoichiometries studied (1:1, 1:2 and 2:1). For the 2:1 anion-to-ligand stoichiometry, $\Delta\left(\Delta G_{tr}^{0',w\to o}\right)$ reaches a constant value of 21.7 kJ mol^{-1} due to the release of two hydroxide anion by anion transfers (see reaction (R11)). $\Delta\left(\Delta G_{tr}^{0',w\to o}\right)$ reaches a constant value at the same concentration ratios where the peak-to-peak potential difference attains a maximum value (see Figs. 3, 5 and 7b) since, at these concentration ratios, the interfacial pH reaches a constant value.

According to the model proposed, we can obtain analytical expressions for relating the formal potential of the anion and the complexes formed, as well as, the half-wave potentials to the initial concentrations of anion and ligand. From Eq. (12), it is easy to show that, for all the transfer mechanisms, the relationship between $\Delta_o^w\phi^{o'}_{[(H_{(n-i)}P)_jL_k]^{ji-}}$ and $\Delta_o^w\phi^{o'}_{H_{(n-i)}P^{i-}}$ can be expressed by [24,25,28]:

$$\Delta_o^w\phi^{o'}_{[(H_{(n-i)}P)_jL_k]^{ji-}} = \Delta_o^w\phi^{o'}_{H_{(n-i)}P^{i-}} + \frac{RT}{jiF}\ln\left[\frac{\beta^o_{ijk}}{\beta^w_{ijk}}(K_{D,L})^k\right] \quad (48)$$

This last relation clearly shows that assisted anion transfer occurs at potential values higher than those of the simple anion transfer, i.e., $\frac{\beta^o_{ijk}}{\beta^w_{ijk}}(K_{D,L})^k > 1$. On this basis, different limiting cases can be recognized for the assisted ion transfer. Shao et al. [45] have proposed a terminology to characterize such cases, based mainly on the comparison of the stability constant of the complex at both phases. The authors have defined three different types of assisted ion transfer mechanisms: aqueous complexation reaction followed by ion transfer (ACT); ion transfer by interfacial complexation (TIC); and ion transfer followed by complexation in the organic phase (TOC). The most frequently observed mechanisms correspond to ACT and TIC types of transfer.

According to the methodology proposed by Matsuda and coworkers for TIC mechanism [24,25], and further generalized by Girault and co-workers for different mechanisms of facilitated ion transfer [28], it is possible to derive general equations that relate the half-wave potential, $\Delta_o^w\phi_{\frac{1}{2}}$, to the initial concentrations of ligand and anion for the BASA model.

We will now consider the mathematical expressions for the half-wave potential of a particular anion *i*. The complexes formed by the anion show a single *j* anion-to-ligand stoichiometry. It is only possible to obtain analytical expressions for two limiting cases:

when $c_L^{init} \gg c_{H_nP}^{init}$ and $c^o_{H_{(n-i)}P^{i-}} \ll \frac{c_{H_nP}^{init}}{2\xi}$,

$$\Delta_o^w\phi^{\frac{1}{2}}_{[(H_{(n-i)}P)_jL_k]^{ji-}} = \Delta_o^w\phi^{0'}_{H_{(n-i)}P^{i-}} + \frac{RT}{jiF}\ln(\xi) + \frac{RT}{iF}\ln\left(\alpha_{H_{(n-i)}P^{i-}}\right) + \frac{RT}{jiF}\ln\left[j\left(\frac{c_{H_nP}^{init}}{2}\right)^{(j-1)}\sum_{k=1}^{l}\beta^o_{ijk}\left(c_L^{init}\right)^k\right] \quad (49)$$

and when $c_L^{init} \ll c_{H_nP}^{init}$

$$\Delta_o^w\phi^{\frac{1}{2}}_{[(H_{(n-i)}P)_jL_k]^{ji-}} = \Delta_o^w\phi^{0'}_{H_{(n-i)}P^{i-}} + \frac{RT}{iF}\ln\left(\alpha_{H_{(n-i)}P^{i-}}\right) + \frac{RT}{iF}\ln\left(c_{H_nP}^{init}\right) + \frac{RT}{jiF}\ln\left[\sum_{k=1}^{l}k\beta^o_{ijk}\left(\frac{c_L^{init}}{2}\right)^{(k-1)}\right] \quad (50)$$

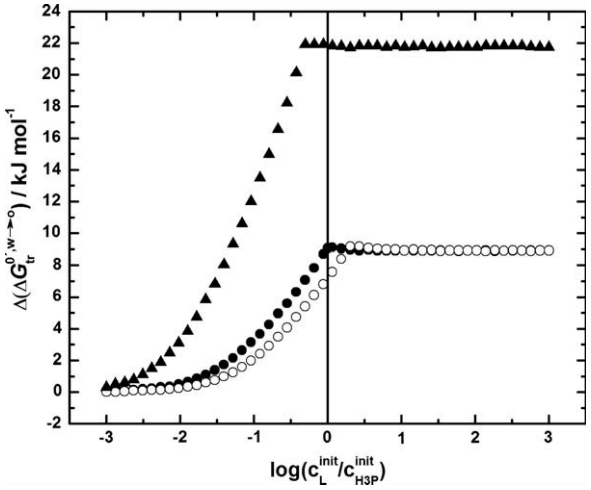

Fig. 8. Change of the free energy transfer defined by Eq. (47) as function of $\log\left(c_L^{init}/c_{H_3P}^{init}\right)$. The change of the free energy transfer results is shown by different anion-to-ligand stoichiometries: 1:1 (filled circle), 1:2 (open circle) and 2:1 (filled triangle up).

where

$$\left(\alpha_{\mathrm{H}_{(n-i)}\mathrm{P}^{i-}}\right)^{-1} = 1 + \sum_{g=1}^{i} \left(c^{\mathrm{w}}_{\mathrm{H}^+}\right)^{g} \left(\prod_{h=i+1-g}^{i} K^{\mathrm{w}}_{\mathrm{a},h}\right)^{-1} + \sum_{g=1}^{n-i} \left(c^{\mathrm{w}}_{\mathrm{H}^+}\right)^{-g} \prod_{h=1}^{g} K^{\mathrm{w}}_{\mathrm{a},(i+h)}$$

When we consider j = 1 and a single anionic form, Eqs. (49) and (50) show a behaviour similar to that described in previous works [24,25,28]. In limiting experimental conditions, the limiting expressions of half-wave potentials obtained with BASA and UBASA models are mutually consistent (see Figs. 3, 5 and 7a). In the case of $c^{\mathrm{init}}_{\mathrm{L}} \gg c^{\mathrm{init}}_{\mathrm{H}_n\mathrm{P}}$, the intercept differs in the energy required to hydrolyze water (Fig. 8).

Another interesting topic is the peak-to-peak potential differences for the stoichiometries analyzed. Under purely diffusion-controlled conditions at a liquid|liquid interface and taking account of that all charge transfer processes analyzed in Section 2 occur by interfacial complexation (TIC/TID mechanism [45]), the maximum value is reached by the following concentration ratio:

$$k^{-1}\chi_{\mathrm{peak,L}}\sqrt{D^{\mathrm{o}}}c^{\mathrm{init}}_{\mathrm{L}} = j^{-1}\chi_{\mathrm{peak,H_3P}}\sqrt{D^{\mathrm{w}}}c^{\mathrm{init}}_{\mathrm{H_3P}} \quad (51)$$

where $\chi_{\mathrm{peak,L}}$ and $\chi_{\mathrm{peak,H_3P}}$ are the dimensionless peak currents for $c^{\mathrm{init}}_{\mathrm{L}} \ll c^{\mathrm{init}}_{\mathrm{H_3P}}$ and $c^{\mathrm{init}}_{\mathrm{L}} \gg c^{\mathrm{init}}_{\mathrm{H_3P}}$, respectively [28]. Both dimensionless peak currents vary with the complexation stoichiometry.

3. Conclusion

A key point in this work is the effect of water autoprotolysis on the facilitated anion transfer across the oil|water interface. General equations were developed for facilitated transfer of anions and three particular cases were systematically analyzed in order to illustrate the effect of the stoichiometry of the complexes formed on the shape of the current–potential profiles. These systems were analyzed considering the maximum contribution of the coupled chemical reactions using a pH for the aqueous phase where HP^{2-} prevails. A systematic analysis of the effect of pH and the concentration ratios for the different complexes formed was performed.

In addition, the half-wave potential dependence on the initial concentration of anion and ligand has been analyzed for a single j anion. The relationships obtained allow determining the stoichiometry and overall association constants of the complexes formed [24,25,28].

It was shown that for unbuffered systems (UBASA model) and experimental conditions that increase coupled chemical reactions; the peak-to-peak potential difference may be substantially greater than that expected according to the charge of the anion transfer.

In the analysis performed in this work, monovalent species were chosen because all the parameters that characterize the charge transfer process, i.e. peak-to-peak potential difference, can be easily translated to polyvalent anions. For systems with monovalent anions, the parameters that characterize the charge transfer process show the maximum variation in all experimental conditions studied. This analysis may yield further insights into the recent experimental results reported by Arrigan and co-workers for the transfer of phosphate anions assisted by a urea-functionalized calix[4]arene ionophore [19]. In the basis of their results, the authors propose that only the monohydrogen phosphate species is being transferred under the experimental conditions studied [19].

Acknowledgements

S.A.D. is a researcher from Consejo Nacional de Investigaciones Científicas y Tecnológicas (CONICET). This work was supported by CONICET and Secretaría de Ciencia y Tecnología (SECyT-UNC). Helpful discussion with N. Wilke and language assistance by C. Mosconi are gratefully acknowledged.

References

[1] J. Koryta, Electrochim. Acta 24 (1979) 293.
[2] H.H. Girault, in: J.O'M. Bockris, B.E. Conway, R.E. White (Eds.), Modern Aspect of Electrochemistry, vol. 25, Plenum Press, New York, 1993, pp. 1–62.
[3] Anion Sensing, I. Stibor (Eds.), Topics in Current Chemistry, vol. 255, Springer-Verlag, Berlin/Heidelberg, 2005.
[4] N. Teramae, S. Nishizawa, A. Yamaguchi, T. Uchida, in: H. Watarai, N. Teramae, T. Sawada (Eds.), Interfacial Nanochemistry – Molecular Science and Engineering at Liquid–Liquid Interfaces, Kluwer Academic Plenum Publishers, New York, 2005, pp. 233–248.
[5] Y. Shao, B. Linton, A.D. Hamilton, S.G. Weber, J. Electroanal. Chem. 441 (1998) 33.
[6] R. Cui, Q. Li, D.E. Gross, X. Meng, B. Li, M. Marquez, R. Yang, J.L. Sessler, Y. Shao, J. Am. Chem. Soc. 130 (2008) 14364.
[7] T. Shioya, S. Nishizawa, N. Teramae, J. Am. Chem. Soc. 120 (1998) 11534.
[8] S. Nishizawa, T. Kamaishi, T. Yokobori, R. Kato, Y.-Y. Cui, T. Shioya, N. Teramae, Anal. Sci. 20 (2004) 1559.
[9] S. Nishizawa, T. Yokobori, R. Kato, K. Yoshimoto, T. Kamaishi, N. Teramae, Analyst 128 (2003) 663.
[10] R. Kato, Y.-Y. Cui, S. Nishizawa, T. Yokobori, N. Teramae, Tetrahedron Lett. 45 (2004) 4273.
[11] K. Shigemori, S. Nishizawa, T. Yokobori, T. Shioya, N. Teramae, New J. Chem. 26 (2002) 1102.
[12] S. Nishizawa, T. Yokobori, T. Shioya, N. Teramae, Chem. Lett. 30 (2001) 1058.
[13] S. Nishizawa, T. Yokobori, R. Kato, T. Shioya, N. Teramae, Bull. Chem. Soc. Jpn. 74 (2001) 2343.
[14] Q. Qian, G.S. Wilson, K. Bowman-James, H.H. Girault, Anal. Chem. 73 (2001) 497.
[15] Q. Qian, G.S. Wilson, K. Bowman-James, Electroanalysis 16 (2004) 1343.
[16] R.A.W. Dryfe, S.S. Hill, A.P. Davis, J.-B. Joos, E.P.L. Roberts, Org. Biomol. Chem. 2 (2004) 2716.
[17] H. Katano, Y. Murayama, H. Tatsumi, Anal. Sci. 20 (2004) 553.
[18] P.J. Rodgers, P. Ping, Y. Kim, S. Amemiya, J. Am. Chem. Soc. 30 (2008) 7436.
[19] F. Kivlehan, W.J. Mace, H.A. Moynihan, D.W.M. Arrigan, Electrochim. Acta 54 (2009) 1919.
[20] N. Katia, R.A. Harries, A.M. Nelly, J.S. Fossey, T.D. James, F. Marken, J. Solid State Electrochem. 13 (2009) 1475.
[21] D. Homolka, K. Holub, V. Marecek, J. Electroanal. Chem. 138 (1982) 29.
[22] T. Kakiuchi, M. Senda, J. Electroanal. Chem. 300 (1991) 431.
[23] T. Kakiuchi, J. Colloid Interface Sci. 156 (1993) 406.
[24] H. Matsuda, Y. Yamada, K. Kanamori, Y. Kudo, Y. Takeda, Bull. Chem. Soc. Jpn. 64 (1991) 1497.
[25] Y. Kudo, Y. Takeda, H. Matsuda, J. Electroanal. Chem. 96 (1995) 333.
[26] P.D. Beattie, R.G. Wellington, H.H. Girault, J. Electroanal. Chem. 396 (1995) 317.
[27] F. Reymond, P.-A. Carrupt, H.H. Girault, J. Electroanal. Chem. 449 (1998) 49.
[28] F. Reymond, G. Lagger, P.-A. Carrupt, H.H. Girault, J. Electroanal. Chem. 451 (1998) 59.
[29] L. Tomaszewski, F. Reymond, P.-F. Brevet, H.H. Girault, J. Electroanal. Chem. 483 (2000) 135.
[30] Y. Kudo, H. Imamizo, K. Kanamori, S. Katsuta, Y. Takeda, H. Matsuda, J. Electroanal. Chem. 509 (2001) 128.
[31] R.A. Iglesias, S.A. Dassie, J. Electroanal. Chem. 533 (2001) 1.
[32] J.I. Garcia, R.A. Iglesias, S.A. Dassie, J. Electroanal. Chem. 580 (2005) 255.
[33] R. Gulaboski, E.S. Ferreira, C.M. Pereira, M.N.D.S. Cordeiro, A. Garau, V. Lippolis, A.F. Silva, J. Phys. Chem. C 112 (2008) 153.
[34] F. Reymond, P.-F. Brevet, P.-A. Carrupt, H.H. Girault, J. Electroanal. Chem. 424 (1997) 121.
[35] S. Sawada, T. Osakai, Phys. Chem. Chem. Phys. 1 (1999) 4819.
[36] T. Osakai, T. Hirai, T. Wakamiya, S. Sawada, Phys. Chem. Chem. Phys. 8 (2006) 985.
[37] S.A. Dassie, J. Electroanal. Chem. 578 (2005) 159.
[38] S.A. Dassie, J. Electroanal. Chem. 585 (2005) 256.
[39] J.I. Garcia, R.A. Iglesias, S.A. Dassie, J. Electroanal. Chem. 586 (2006) 225.
[40] R.S. Nicholson, I. Shain, Anal. Chem. 36 (1964) 706.
[41] F. Reymond, G. Steyaert, P.-A. Carrupt, B. Testa, H.H. Girault, Helv. Chim. Acta 76 (1996) 101.
[42] W.H. Press, S.A. Teukolsky, I.T. Vetterling, B.P. Flannery, Numerical Recipes in Fortran 77. The Art of Scientific Computing, second ed., Cambridge University Press, 1992. pp. 340–376.
[43] R.L. Burden, J.D. Douglas Faires, Análisis Numérico, Grupo Editorial Iberoamérica (Ed.), México, 1985, pp. 531–556.
[44] Subroutines in Fortran are free available in <http://www.netlib.org>.
[45] Y. Shao, M.D. Osborne, H.H. Girault, J. Electroanal. Chem. 318 (1991) 101.